Available online at www.sciencedirect.com

ScienceDirect

journal homepage: www.elsevier.com/locate/he

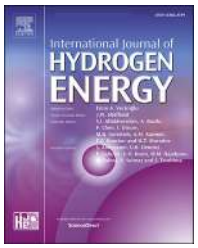

Cu–Fe–Al–O mixed spinel oxides as oxygen carrier for chemical looping hydrogen generation

Dongxu Cui [1], *Yu Qiu* [1], *Min Li, Li Ma, Shuai Zhang, Dewang Zeng* [*], *Rui Xiao* [**]

Key Laboratory of Energy Thermal Conversion and Control of Ministry of Education, School of Energy and Environment, Southeast University, Nanjing 210096, PR China

HIGHLIGHTS

- A mixed spinel $Cu_{0.2}Fe_{0.8}(FeAl)O_x$ material is synthesized as an oxygen carrier.
- It performs a good redox stability even at reduction level of 0.75 during 20 cycles.
- The spinel support can inhibit sintering of Cu and Fe active compositions.

ARTICLE INFO

Article history:
Received 30 December 2019
Received in revised form
11 February 2020
Accepted 22 February 2020
Available online 12 March 2020

Keywords:
Chemical looping
Redox stability
Hydrogen yield
Sintering

ABSTRACT

The reduction level for a metal oxides carrier determines the final hydrogen yield for a chemical looping hydrogen generation process. Nevertheless, when the oxygen carrier is reduced at a high level, the sintering of materials would be accelerated. In this paper, we prepare a $Cu_{0.2}Fe_{0.8}(FeAl)O_x$ spinel material and investigate its hydrogen production performance. The results indicate that it exhibits a good redox stability even at reduction level of 0.75 during 20 cycles. In contrast, the deactivation of Fe_2O_3 oxygen carrier can be obviously observed in the first few cycles. This enable the material with stable hydrogen production at a high yield about 7 mmol/g, which is 3.5 times higher than that of Fe_2O_3. Upon SEM and XRD characterization techniques, we find that the reason of the both good stability and high hydrogen yield is that the ability of spinel support to inhibit sintering of Cu and Fe active compositions.

Introduction

Hydrogen is identified as the most promising and cleanest energy carrier because it has a high energy density of 120.7 kJ/g and only produce water during utilization process [1,2]. Hydrogen is defined as an energy carrier rather than a resource, since it is mainly stored in water. Much primary energy sources would be consumed to produce hydrogen [3,4]. At present, most of hydrogen is produced by steam methane reforming technology (SMT) in industrial. However, to obtain pure hydrogen, multiple reactors and pressure swing adsorption processes are employed, resulting in the system of SMT becomes complex. In addition, much methane would be consumed to provide heat for water-gas shift and the coke

* *Corresponding author.*
** *Corresponding author.*
E-mail addresses: dwzeng@seu.edu.cn (D. Zeng), ruixiao@seu.edu.cn (R. Xiao).
[1] These people contributed equally to this work.
https://doi.org/10.1016/j.ijhydene.2020.02.145

deposition would cause catalyst deactivation, which increases operating costs [5,6]. For the purpose of making it feasible that H_2 becomes an energy carrier, an efficient method to produce pure hydrogen is indispensable and desirable.

The chemical looping water spitting (CLWS) is a promising hydrogen generation technology. The CLWS technology can produce pure hydrogen without any energy penalty for purification and system of CLWS is simple [7]. Synthesis gas or carbon dioxide capture can be achieved simultaneously with the hydrogen production process in CLWS [8]. The achievement of chemical looping depends on oxygen carrier, which usually is metal oxides transferring oxygen by phase transition. A typical CLWS procedure can be described by following steps. Firstly, oxygen carrier is reduced to oxygen-depleted stages by fuel (*e.g.* methane, CO, coal, and biomass, etc.), meanwhile, the fuel is oxidized [9,10]. Then the oxygen-depleted oxygen carrier is conveyed to steam reactor. In this reactor oxygen carrier is re-oxidized and steam is split to hydrogen simultaneously. The hydrogen is the only gas product in this process after condensing steam [11].

The key to the chemical looping approach is the selection and operation of the oxygen carrier materials. In recent years, a series of metal oxides (*e.g.* Fe_2O_3 [12–14], Co_3O_4 [15,16], and Mn_2O_3 [17,18]) have been intensively tested. Among these materials iron oxide is the most promising one due to the good compatibility to environment, low costs, good mechanical strength, and high oxygen storage capacity [14,19]. In terms of the associated redox reaction of iron oxides for CLWS, two major cycles are involved according to the different reduction level. Two mainly pathways for hydrogen production are Fe–> FeO and FeO–> Fe_3O_4 [20]. The former pathway is 1.5 times hydrogen yield than the second one, indicating solid flux or material usage can be decreased to a quarter in a fluidized or fixed bed system.

Unfortunately, the significant deactivation can be tested when oxygen carrier is operated at a high reduction level, which has been reported by some authors. Bohn et al. studied redox stability of pure iron oxides with several reduction levels at 900 °C in a typical chemical looping hydrogen production process [21]. They found that oxygen carrier kept a good reactivity over 10 cycles, when the oxygen carrier with a low reduction level cycled between phase Fe_2O_3 and FeO. However, the hydrogen yield plunged after first redox cycle when the oxygen carrier was operated at a high reduction level cycling between Fe_2O_3 and Fe. Bleeker et al. also found similar results via testing the surface area change of iron oxide oxygen carrier in various cycles [22]. The surface area of the fresh oxygen carrier was 31 m^2/g but it diminished to 0.37 m^2/g after 14 cycles, when the phase transition of oxygen carrier was between Fe_2O_3 and Fe. Diego et al. reported the mechanism of these processes [23]. Because the density of Fe was much higher than that of FeO, Fe_3O_4 and Fe_2O_3, the higher lattice stress would appear when iron oxides was reduced to Fe metal. This lattice stress would damage the initial structure of oxygen carrier, causing severe sintering.

In order to prevent material from sintering and improve redox stability, many inert metal oxides are employed as support materials, such as Al_2O_3 [5,24], CeO_2 [25], ZnO [26,27], MgO [28,29], ZrO_2 [3,30], and SiO_2 [31,32]. These supports as physical barriers prevent active iron atom from aggregation and sintering, improving redox stability of oxygen carrier [33,34]. However, the inert supports addition would change oxygen storage capacity and reactivity of oxygen carrier. The interaction of active and inert components cannot be ignored leading to forming a new inert spinel structure, when reaction temperature is high enough [35]. The new spinel material would perform a different physical and chemical properties with the original material.

Here, we prepared a $Cu_{0.2}Fe_{0.8}(FeAl)O_x$ spinel material as an oxygen carrier and studied the redox stability at various reduction levels (C is defined as the proportion of actual weight loss to that of fully reduction, C = 0.25, 0.5, 0.75 and 1) in a typical chemical looping hydrogen production process. Compared with Fe_2O_3, the $Cu_{0.2}Fe_{0.8}(FeAl)O_x$ showed a better redox stability at high reduction level.

Experiments

Synthesis of the $Cu_{0.2}Fe_{0.8}(FeAl)O_x$ materials

The sol-gel method was used to prepare $Cu_{0.2}Fe_{0.8}(FeAl)O_x$ material. Typically, the $Cu(NO_3)_2$, $Fe(NO_3)_3$, and $Al(NO_3)_3$ metal nitrates were dissolved in 100 ml pure water with molar ratio of 0.2:1:1. Based on molar ratio of Fe^{3+}:Fe^{2+} of 1:0.8, the $FeCl_2$ was added to mixed solution. The polyethylene glycol and citric acid then were added to the mixed solution with 1:4 M ratio and stirred in 110 °C oil bath for 16 h until it became thick gel. The molar proportion of citric acid and metal cation was 1.2:1. At last, the gel precursor was calcined at 500 °C (10 °C/min) for 2 h and then to 1000 °C (10 °C/min) for 2 h at air atmosphere. The $CuAl_2O_4$, $FeAl_2O_4$, $CuFe_2O_4$, and Fe_2O_3 were also synthesized by the sol-gel method for reference.

Material characterization

In order to characterize the crystalline phases of the oxygen carriers, X-ray diffraction (XRD) samples were implemented using Rigaku SmartLab 9 diffractometer in the range of (2θ) 10° to 80°. The HORIBA Evolution spectrometer (Raman spectra) with a 532 nm He/Ne laser source was also employed to characterize the material crystalline structure. The scanning electron microscopy (SEM) was performed to investigate surface morphology of the materials. The FEI 400FEG electron microscope was used to observe oxygen carriers which were pretreated by spray gold. Temperature program reduction (TPR) with a thermal conductivity detector (TCD) was implemented using FineSorb-3010 equipment. The 20 mg sample was first pretreated under He atmosphere at 200 °C. After the reactor cooled to room temperature, 10% hydrogen was employed as reduction agent at a gas rate of 20 ml/min from room temperature to 900 °C with a ramp rate of 10 °C/min.

The redox reactivity and phase transition of the $Cu_{0.2}Fe_{0.8}(FeAl)O_x$ oxygen carrier were investigated in thermogravimetric analyzer (TGA) with 5% CO at 700 °C. CO_2 was used as an oxidation agent for simulated steam. Finally, air was fed into thermogravimetric analyzer and N_2 was used as purge gas. All gas flow rates were 50 ml/min.

Chemical looping tests

The 0.5 g $Cu_{0.2}Fe_{0.8}(FeAl)O_x$ oxygen carrier was reduced by 5% carbon monoxide. Subsequently, it was oxidized by 30% steam and air with the gas flow rates of 1200 ml/min in a 12 mm inner diameter fixed bed reactor at 600, 700, 800, and 900 °C. The outlet gases were detected by MRU gas analyzer. The hydrogen yield and oxygen carrier reduction level were calculated by mole of carbon dioxide and hydrogen in produce gases. The details of experimental process can acquire from our former study [36].

Results and discussion

Material characterization

The XRD patterns of $Cu_{0.2}Fe_{0.8}(FeAl)O_x$ is illustrated in Fig. 1, of which the main diffraction peaks locate at 30.8°, 36.4° and 44.1°. The lattice parameter of $Cu_{0.2}Fe_{0.8}(FeAl)O_x$ was 8.17 Å. For research the crystalline structure of this material, $FeAl_2O_4$, $CuAl_2O_4$, and $CuFe_2O_4$ (AB_2O_4) spinel materials were prepared as references with the lattice parameter of 8.15 Å ($FeAl_2O_4$, PDF: 34–0192), 8.08 Å ($CuAl_2O_4$, PDF: 33–0448), and 8.35 Å ($CuFe_2O_4$, PDF: 25–0283), respectively. Because the cation radius of A site Cu^{2+} (0.073 nm) and B site Al^{3+} (0.068 nm) are lower than that of Fe^{2+} (0.077 nm) and Fe^{3+} (0.069 nm), the lattice parameter increase of $Cu_{0.2}Fe_{0.8}(FeAl)O_x$ can be attributed to the A site Cu^{2+} cation and B site Al^{3+} cation were partial replaced by Fe^{2+} and Fe^{3+} in the original $CuAl_2O_4$ spinel structure. Therefore, it can infer that the $Cu_{0.2}Fe_{0.8}(FeAl)O_x$ material was formed from partial cations substitution.

Fig. 2 shows the Raman spectrum of the $Cu_{0.2}Fe_{0.8}(FeAl)O_x$ oxygen carrier, where five main peaks were observed. The Oh-site mode situated at ~219, ~400 and ~494 cm^{-1} corresponding to the octahedral sublattice structure and Td-site mode located at ~603 and ~723 cm^{-1} corresponding to the tetrahedral sublattice structure [37]. It can conclude that based on the group theory the oxygen carrier was a pure $Cu_{0.2}Fe_{0.8}(FeAl)O_x$ cubic inverse spinel structure from the Raman spectrum.

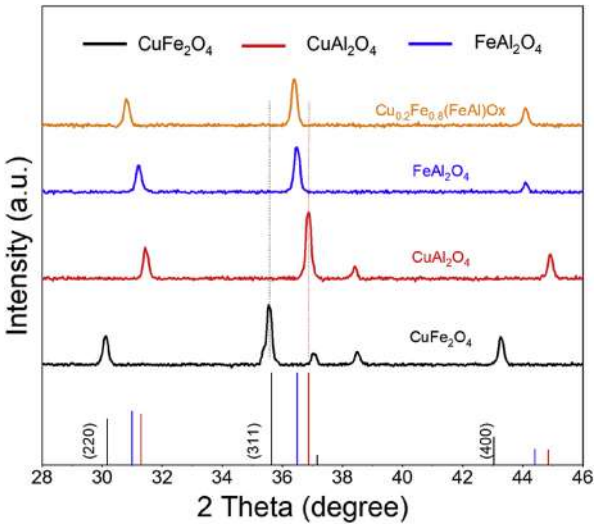

Fig. 1 – XRD patterns of the prepared $Cu_{0.2}Fe_{0.8}(FeAl)O_x$ material. The crystalline patterns correspond to $CuAl_2O_4$(vertical red lines), $FeAl_2O_4$(vertical blue lines) and $CuFe_2O_4$ (vertical black lines), respectively.

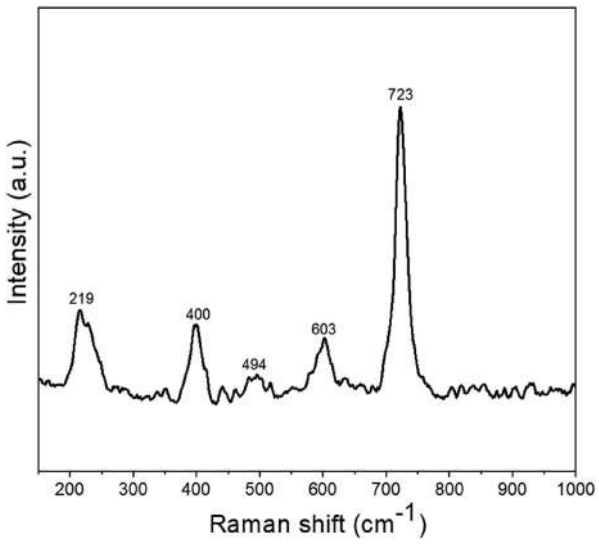

Fig. 2 – The Raman spectra of the as-prepared $Cu_{0.2}Fe_{0.8}(FeAl)O_x$ oxygen carrier.

Reactivity tests

The hydrogen temperature programmed reduction (TPR) profiles of Fe_2O_3 and $Cu_{0.2}Fe_{0.8}(FeAl)O_x$ are illustrated in Fig. 3. The loosely bonded oxygen on the surface of oxygen carrier would generate the initial low temperature reduction peak and the lattice oxygen of bulk phase would produce the reduction peaks of high temperature [38]. Compared with the pure Fe_2O_3, $Cu_{0.2}Fe_{0.8}(FeAl)O_x$ oxygen carrier showed four

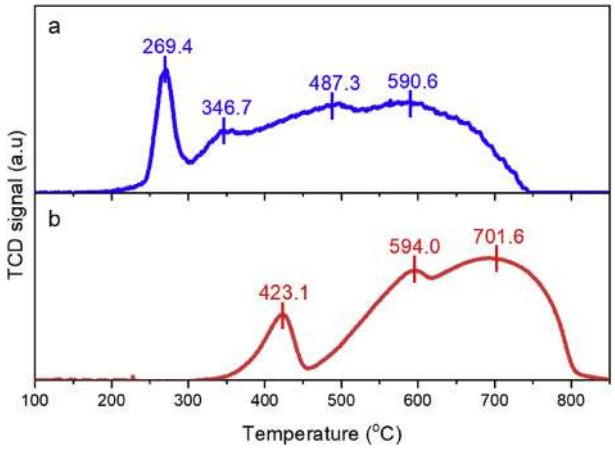

Fig. 3 – TPR curves of the prepared materials. (a) $Cu_{0.2}Fe_{0.8}(FeAl)O_x$ (b) Fe_2O_3.

main reduction peaks at 269.4 °C, 346.7 °C, 487.3 °C, and 590.6 °C [39]. The temperature of initial reduction peak was lower than that of Fe_2O_3, which can be contribute to Cu oxide reduction. In addition, the $Cu_{0.2}Fe_{0.8}(FeAl)O_x$ oxygen carrier was nearly fully reduced at ~750 °C which was lower than that of Fe_2O_3, suggesting that the lattice oxygen of the material can be absolutely released in that temperature and the Cu dopant can obviously improve the lattice oxygen reactivity of iron oxide.

According to the TPR results, the fully reduction temperature of $Cu_{0.2}Fe_{0.8}(FeAl)O_x$ oxygen carrier was nearly 750 °C. For further study the reactivity in a typical CLWS process, the $Cu_{0.2}Fe_{0.8}(FeAl)O_x$ oxygen carrier was investigated in a fixed bed reactor with 600, 700, 800, and 900 °C. As a contrast, the Fe_2O_3 oxygen carrier was also tested in various temperature. As is shown in Fig. 4, high hydrogen production rate of two materials can be found at 900 °C. The hydrogen production rate and yield deteriorated with the decrease of the reaction temperatures. When the temperature dropped from 900 to 700 °C, the hydrogen yield of the iron oxide sample decreased by a quarter. But the hydrogen yield of $Cu_{0.2}Fe_{0.8}(FeAl)O_x$ oxygen carrier was still nearly 10 mmol/g, which was not obviously changed with temperature decrease. As temperature further decrease to 600 °C, the plunge of hydrogen yield can be noticed in $Cu_{0.2}Fe_{0.8}(FeAl)O_x$ sample. It can be deduced that Cu dopant effectively improved the reactivity of the lattice oxygen and further lowered the reaction temperature.

Redox stability in chemical looping process

Some authors have reported that the severe deactivation would appear when oxygen carrier was operated at a high reduction level [40]. Therefore, the $Cu_{0.2}Fe_{0.8}(FeAl)O_x$ oxygen carrier was tested with several reduction levels in a fixed bed reactor. As a contrast, Fe_2O_3 oxygen carrier was also tested. The reduction levels are got by calculated the amount of carbon dioxide product in reduction process. Therefore, the oxygen carrier was first fully reduced. Then the CO reduction time of each reduction levels were confirmed for the next cycle tests. The reduction time was fixed for one of reduction level.

Typically, as is shown in Fig. 5, both two oxygen carriers performed good redox stability during the whole 20 cycles with the reduction level of 0.25. But the hydrogen yield was both lower than 2 mmol/g. As the reduction level raised, the hydrogen yield of both two oxygen carriers increased at first cycle but the Fe_2O_3 was rapidly deactivated in following cycles. But the $Cu_{0.2}Fe_{0.8}(FeAl)O_x$ exhibited a better redox stability than Fe_2O_3. The hydrogen yield of $Cu_{0.2}Fe_{0.8}(FeAl)O_x$ and Fe_2O_3 was 7.69 mmol/g and 5.19 mmol/g under reduction level of 0.75 at the first cycle. After 20 cycles, the $Cu_{0.2}Fe_{0.8}(FeAl)O_x$ material remained a high hydrogen yield of 7.05 mmol/g but it diminished to 1.9 mmol/g for Fe_2O_3. These results revealed that $Cu_{0.2}Fe_{0.8}(FeAl)O_x$ material can keep a good stability even at reduction level of 0.75 suggesting that the less materials usage in a fixed bed reactor or solid flux in a fluidized reactor can be implemented.

Mechanism study

For further exploration of the above results mechanism, the material was tested in TG analyzer. The various reaction stages of oxygen carrier were characterized by X-ray diffraction. The phase transition of the oxygen carrier was confirmed by weight loss and XRD patterns in a chemical looping cycle.

Fig. 6 shows the TG curve combined with XRD patterns, the spinel diffraction peaks could be found and the Cu metal diffraction peak can be observed since the initial reduction minutes, indicating the Cu metal was firstly exsolved from the spinel support and phase transitions of support material were between different spinel. With further reduction of CO, the intensity of the spinel peaks gradually decreased, the Cu metal diffraction peak was no change, suggesting the Cu was absolutely exsolved from spinel support. Thereby the material generally converted to the formation of $Cu^0/FeAlO_x$ spinel. In addition, the diffraction peak of Fe metal was noticed and gradually increased in later reduction stages. It can be concluded that the active compositions of Cu and Fe in the spinel were gradually exsolved from the support spinel in the reduction process. In fully reduction stage, only metallic peaks

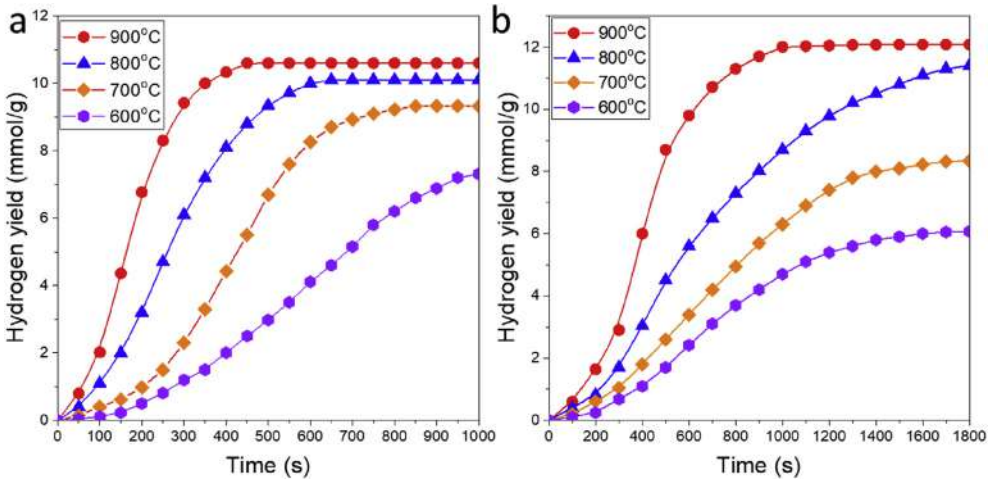

Fig. 4 – The time-varying hydrogen yield of (a) $Cu_{0.2}Fe_{0.8}(FeAl)O_x$ (b) Fe_2O_3 at various temperatures.

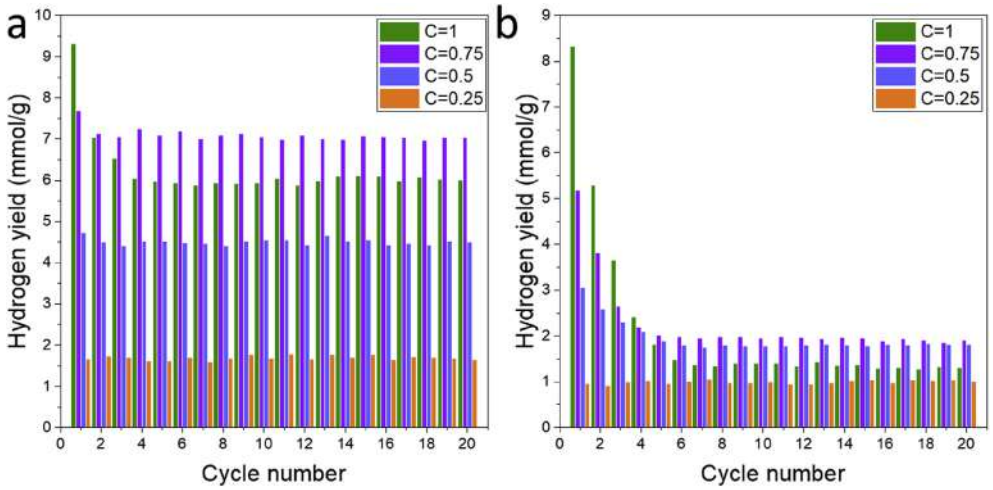

Fig. 5 – The hydrogen yield of (a) $Cu_{0.2}Fe_{0.8}(FeAl)O_x$ and (b) Fe_2O_3 with various reduction levels at 700 °C during 20 cycles.

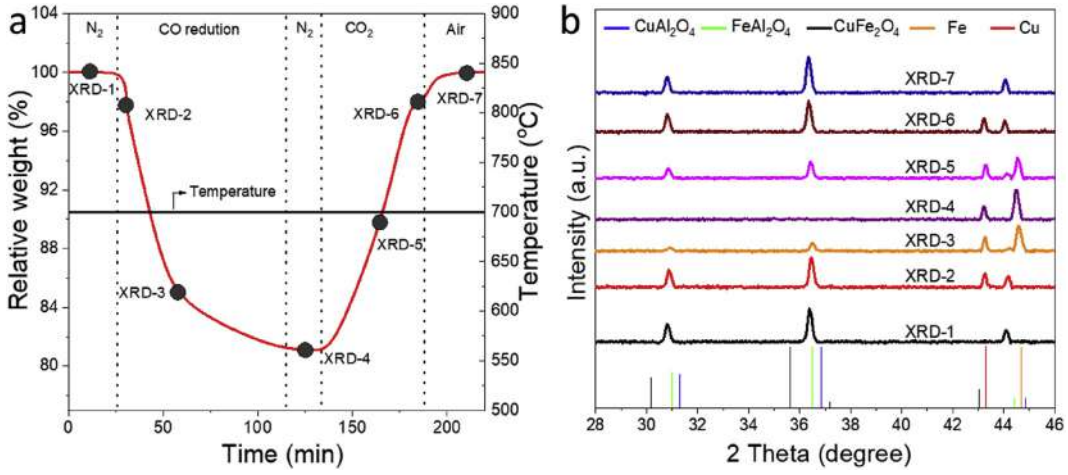

Fig. 6 – (a) The TG curve of $Cu_{0.2}Fe_{0.8}(FeAl)O_x$ material with CO reduction, CO_2 and air oxidation at 700 °C. (b) The XRD patterns of $Cu_{0.2}Fe_{0.8}(FeAl)O_x$ material corresponding to TG curve in various stages.

can be observed and no spinel characteristic peaks could be detected. The absence of Al element was possibly that Al_2O_3 existed in an amorphous state. So the material phase was Cu^0Fe^0/Al_2O_3 after full reduction.

In subsequently, the Cu^0Fe^0/Al_2O_3 oxygen carrier was re-oxidized by CO_2. Fig. 6b shows that the Fe metal was rapidly dissolved into Al_2O_3 and formed a spinel structure, which can be deduced from spinel diffraction peaks. And the Cu metal was also dissolved into the $FeAlO_x$ spinel support in air oxidation stage. After air oxidation other peaks all disappeared except spinel diffraction peaks, indicating the oxygen carrier regenerated back to initial spinel structure.

Following the phase transition analysis, the phase of $Cu_{0.2}Fe_{0.8}(FeAl)O_x$ oxygen carrier in each reduction and oxidation stages was characterized by XRD at 1st, 5th, 10th and 20th cycles under reduction level of 0.25, 0.5, 0.75, and 1. It can be observed in Fig. 7 that the phase transition was reversible in all cases. But there were two different cycle systems. One was the oxygen carrier was fully reduced to Cu^0Fe^0 metal and Al_2O_3 phases (Fig. 7a). Another one was the oxygen carrier partial reduced to Cu^0Fe^0 metal and spinel phase (Fig. 7b, c, and d). But when it comes to complete reduction, as cycle number grew, the metal diffraction peak became weaker, indicating the part of spinel was not reducible in the same CO reduction times. The aggregation and growth of the crystalline spinel phase inhibited the bulk lattice oxygen diffusion. It can be deduced that the spinel support can inhibit the aggregation and sintering of the active phase.

The Scherrer equation was used to calculate crystallite size of oxygen carrier in various cycles (Fig. 8). The crystallite size of oxygen carrier was lower than 55 nm when the reduction

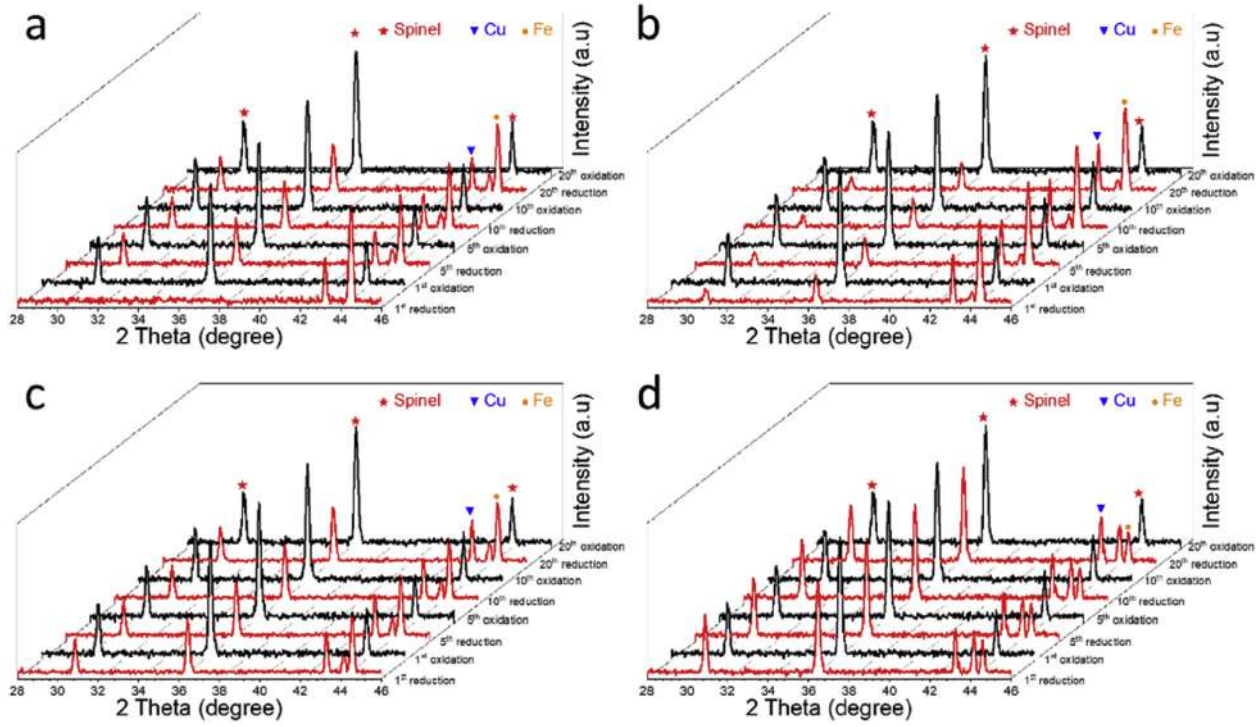

Fig. 7 – The XRD patterns of $Cu_{0.2}Fe_{0.8}(FeAl)O_x$ oxygen carrier with various reduction levels at 700 °C. (a) C = 1 (b) C = 0.75 (c) C = 0.5 (d) C = 0.25 at 1st, 5th, 10th and 20th cycles.

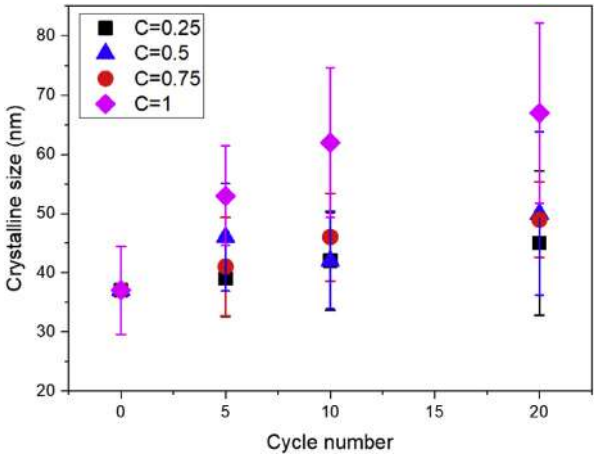

Fig. 8 – The crystallite size evolution of $Cu_{0.2}Fe_{0.8}(FeAl)O_x$ oxygen carrier with various reduction levels at 700 °C.

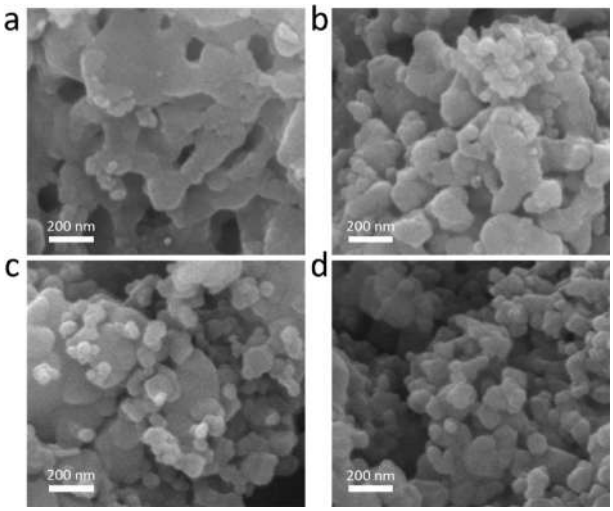

Fig. 9 – The SEM images of $Cu_{0.2}Fe_{0.8}(FeAl)O_x$ oxygen carrier with various reduction levels at 700 °C. (a) C = 1 (b) C = 0.75 (c) C = 0.5 (d) C = 0.25 after 20 cycles.

level was less than 0.75. In addition, as cycle number increase, crystallite size did not obviously increase. In contrast, the grain size of oxygen carrier, which was fully reduced and oxidized, rapidly increased to nearly 65 nm. The oxygen carrier cannot be fully reduced at the same reduction time, resulting in the hydrogen yield decrease. Fig. 9 shows the surface morphology of the $Cu_{0.2}Fe_{0.8}(FeAl)O_x$ oxygen carrier which cycled with various reduction level. The obvious aggregation and sintering of particle can be observed, when the oxygen carrier was cycling with fully reduction and oxidation (C = 1), which agreed with the XRD results.

Conclusion

In this study, we synthesized a $Cu_{0.2}Fe_{0.8}(FeAl)O_x$ spinel material for chemical looping hydrogen production and

investigated its reactivity and redox stability at different temperatures and several reduction levels. As the material characterization results of XRD and Raman spectra, the $Cu_{0.2}Fe_{0.8}(FeAl)O_x$ material showed a pure cubic inverse spinel structure. In TPR and fixed bed tests, this spinel material exhibited a higher reactivity than Fe_2O_3 sample. In addition, it performed a high redox stability and hydrogen yield with reduction level of 0.75 in prolonged fixed bed tests. The mechanism research showed the active phase of Cu and Fe exsolved from the support in reduction stage, and dissolved into the support during oxidation process. And the spinel support can inhibit migration and aggregation of the active phase to improve redox stability. The oxygen carrier stable operating at a high reduction level can not only ensure a high hydrogen yield but also can effectively reduce material loading or circulating flow rate in practical fixed or fluidized bed.

Acknowledgements

The authors gratefully acknowledge the National Natural Science Foundation of China (Grant No. 51906041), the Natural Science Foundation of Jiangsu Province (Grant No. BK20190360) and National Science Foundation for Distinguished Young Scholars of China (Grant No. 51525601).

REFERENCES

[1] De Vos Y, Jacobs M, Van Driessche I, et al. Processing and characterization of Fe-based oxygen carriers for chemical looping for hydrogen production. Int J Greenh gas Contr 2018;70:12–21.
[2] Liao M, Chen Y, Cheng Z, et al. Hydrogen production from partial oxidation of propane: effect of SiC addition on Ni/Al2O3 catalyst. Appl Energy 2019:252.
[3] Liu W, Dennis JS, Scott SA. The effect of addition of ZrO2to Fe2O3for hydrogen production by chemical looping. Ind Eng Chem Res 2012;51:16597–609.
[4] Chiron F-X, Patience GS. Kinetics of mixed copper–iron based oxygen carriers for hydrogen production by chemical looping water splitting. Int J Hydrogen Energy 2012;37:10526–38.
[5] Hafizi A, Rahimpour MR, Hassanajili S. Calcium promoted Fe/Al2O3 oxygen carrier for hydrogen production via cyclic chemical looping steam methane reforming process. Int J Hydrogen Energy 2015;40:16159–68.
[6] Wang C, Dou B, Jiang B, et al. Sorption-enhanced steam reforming of glycerol on Ni-based multifunctional catalysts. Int J Hydrogen Energy 2015;40:7037–44.
[7] Rydén M, Arjmand M. Continuous hydrogen production via the steam–iron reaction by chemical looping in a circulating fluidized-bed reactor. Int J Hydrogen Energy 2012;37:4843–54.
[8] Mehrpooya M, Sharifzadeh MMM, Rajabi M, et al. Design of an integrated process for simultaneous chemical looping hydrogen production and electricity generation with CO2 capture. Int J Hydrogen Energy 2017;42:8486–96.
[9] Deng GX, Li KZ, Gu ZH, et al. Synergy effects of combined red muds as oxygen carriers for chemical looping combustion of methane. Chem Eng J 2018;341:588–600.
[10] Luo M, Yi Y, Wang S, et al. Review of hydrogen production using chemical-looping technology. Renew Sustain Energy Rev 2018;81:3186–214.
[11] Dueso C, Thompson C, Metcalfe I. High-stability, high-capacity oxygen carriers: iron oxide-perovskite composite materials for hydrogen production by chemical looping. Appl Energy 2015;157:382–90.
[12] Galvita V, Hempel T, Lorenz H, et al. Deactivation of modified iron oxide materials in the cyclic water gas shift process for CO-free hydrogen production. Ind Eng Chem Res 2008;47:303–10.
[13] Liu T, Yu ZL, Li G, et al. Performance of potassium-modified Fe2O3/Al2O3 oxygen Carrier in coal-direct chemical looping hydrogen generation. Int J Hydrogen Energy 2018;43:19384–95.
[14] Ma SW, Chen SY, Soomro A, et al. Effects of supports on hydrogen production and carbon deposition of Fe-based oxygen carriers in chemical looping hydrogen generation. Int J Hydrogen Energy 2017;42:11006–16.
[15] Hafizi A, Rahimpour MR, Heravi M. Experimental investigation of improved calcium-based CO2 sorbent and Co3O4/SiO2 oxygen carrier for clean production of hydrogen in sorption-enhanced chemical looping reforming. Int J Hydrogen Energy 2019;44:17863–77.
[16] Li M, Zhao K, Zhao ZL, et al. Enhanced hydrogen-rich syngas generation in chemical looping methane reforming using an interstitial doped La1.6Sr0.4FeCoO6. Int J Hydrogen Energy 2019;44:10250–64.
[17] Galinsky N, Mishra A, Zhang J, et al. Ca1–A MnO3 (A = Sr and Ba) perovskite based oxygen carriers for chemical looping with oxygen uncoupling (CLOU). Appl Energy 2015;157:358–67.
[18] Parishan S, Littlewood P, Arinchtein A, et al. Chemical looping as a reactor concept for the oxidative coupling of methane over the Mn x O y -Na 2 WO 4/SiO 2 catalyst, benefits and limitation. Catal Today 2018;311:40–7.
[19] Zhu X, Wei Y, Wang H, et al. Ce–Fe oxygen carriers for chemical-looping steam methane reforming. Int J Hydrogen Energy 2013;38:4492–501.
[20] Zeng L, Cheng Z, Fan JA, et al. Metal oxide redox chemistry for chemical looping processes. Nat Rev Chem 2018;2:349–64.
[21] Bohn CD, Muller CR, Cleeton JP, et al. Production of very pure hydrogen with simultaneous capture of carbon dioxide using the redox reactions of iron oxides in packed beds. Ind Eng Chem Res 2008;47:7623–30.
[22] Bleeker MF, Kersten SRA, Veringa HJ. Pure hydrogen from pyrolysis oil using the steam-iron process. Catal Today 2007;127:278–90.
[23] Alvarez D, Abanades JC. Pore-size and shape effects on the recarbonation performance of calcium oxide submitted to repeated calcination/recarbonation cycles. Energy Fuels 2005;19:270–8.
[24] Imtiaz Q, Yüzbasi NS, Abdala PM, et al. Development of MgAl2O4-stabilized, Cu-doped, Fe2O3-based oxygen carriers for thermochemical water-splitting. J Mater Chem A 2016;4:113–23.
[25] Galvita VV, Poelman H, Bliznuk V, et al. CeO2-modified Fe2O3 for CO2 utilization via chemical looping. Ind Eng Chem Res 2013;52:8416–26.
[26] Liu G, Liao Y, Wu Y, et al. Enhancement of Ca2Fe2O5 oxygen carrier through Mg/Al/Zn oxide support for biomass chemical looping gasification. Energy Convers Manag 2019;195:262–73.
[27] Wang Y, Kattel S, Gao W, et al. Exploring the ternary interactions in Cu-ZnO-ZrO2 catalysts for efficient CO2 hydrogenation to methanol. Nat Commun 2019;10:1166.
[28] Yusuf S, Neal L, Bao Z, et al. Effects of sodium and tungsten promoters on Mg6MnO8-based core–shell redox catalysts for chemical looping—oxidative dehydrogenation of ethane. ACS Catal 2019;9:3174–86.
[29] Cheng Z, Baser DS, Nadgouda SG, et al. C2 selectivity enhancement in chemical looping oxidative coupling of methane over a Mg–Mn composite oxygen carrier by Li-Doping-Induced oxygen vacancies. ACS Energy Lett 2018;3:1730–6.

[30] Hosseini D, Donat F, Kim SM, et al. Redox-driven restructuring of FeMnZr-oxygen carriers enhances the purity and yield of H2 in a chemical looping process. ACS Appl Energy Mater 2018;1:1294–303.
[31] Wang P, Zhao G, Liu Y, et al. TiO 2 -doped Mn 2 O 3 -Na 2 WO 4/SiO 2 catalyst for oxidative coupling of methane: solution combustion synthesis and MnTiO 3 -dependent low-temperature activity improvement. Appl Catal, A 2017;544:77–83.
[32] Yunarti RT, Gu S, Choi J-W, et al. Oxidative coupling of methane using Mg/Ti-doped SiO2-supported Na2WO4/Mn catalysts. ACS Sustainable Chem Eng 2017;5:3667–74.
[33] Ma Z, Zhang S, Xiao R. Insights into the relationship between microstructural evolution and deactivation of Al2O3 supported Fe2O3 oxygen carrier in chemical looping combustion. Energy Convers Manag 2019;188:429–37.
[34] Duan C, Huo J, Li F, et al. Ultrafast room-temperature synthesis of hierarchically porous metal–organic frameworks by a versatile cooperative template strategy. J Mater Sci 2018;53:16276–87.
[35] Zhang L, Wu Y. Sol-gel synthesized MagneticMnFe2O4Spinel ferrite nanoparticles as novel catalyst for oxidative degradation of methyl orange. J Nanomater 2013;2013:1–6.
[36] Zeng D, Qiu Y, Peng S, et al. Enhanced hydrogen production performance through controllable redox exsolution within CoFeAlOx spinel oxygen carrier materials. J Mater Chem A 2018;6:11306–16.
[37] Penke YK, Anantharaman G, Ramkumar J, et al. Aluminum substituted nickel ferrite (Ni-Al-Fe): a ternary metal oxide adsorbent for arsenic adsorption in aqueous medium. RSC Adv 2016;6:55608–17.
[38] Cheng F, Dupont V, Twigg MV. Temperature-programmed reduction of nickel steam reforming catalyst with glucose. Appl Catal, A 2016;527:1–8.
[39] Qiu Y, Zhang S, Cui D, et al. Enhanced hydrogen production performance at intermediate temperatures through the synergistic effects of binary oxygen carriers. Appl Energy 2019:252.
[40] Cui D, Qiu Y, Lv Y, et al. A high-performance oxygen carrier with high oxygen transport capacity and redox stability for chemical looping combustion. Energy Convers Manag 2019;202.